© 2019. Published by The Company of Biologists Ltd | Development (2019) 146, dev171686. doi:10.1242/dev.171686

HUMAN DEVELOPMENT

TECHNIQUES AND RESOURCES ARTICLE

Reproducibility and staging of 3D human retinal organoids across multiple pluripotent stem cell lines

Elizabeth E. Capowski[1], Kayvan Samimi[2], Steven J. Mayerl[1,3,4], M. Joseph Phillips[1,4], Isabel Pinilla[5,6], Sara E. Howden[7,8], Jishnu Saha[1], Alex D. Jansen[1], Kimberly L. Edwards[1], Lindsey D. Jager[1], Katherine Barlow[1], Rasa Valiauga[1], Zachary Erlichman[1], Anna Hagstrom[1], Divya Sinha[1,4], Valentin M. Sluch[9], Xitiz Chamling[9], Donald J. Zack[9], Melissa C. Skala[2,10] and David M. Gamm[1,4,11,*]

ABSTRACT

Numerous protocols have been described for producing neural retina from human pluripotent stem cells (hPSCs), many of which are based on the culture of 3D organoids. Although nearly all such methods yield at least partial segments of retinal structure with a mature appearance, variabilities exist within and between organoids that can change over a protracted time course of differentiation. Adding to this complexity are potential differences in the composition and configuration of retinal organoids when viewed across multiple differentiations and hPSC lines. In an effort to understand better the current capabilities and limitations of these cultures, we generated retinal organoids from 16 hPSC lines and monitored their appearance and structural organization over time by light microscopy, immunocytochemistry, metabolic imaging and electron microscopy. We also employed optical coherence tomography and 3D imaging techniques to assess and compare whole or broad regions of organoids to avoid selection bias. Results from this study led to the development of a practical staging system to reduce inconsistencies in retinal organoid cultures and increase rigor when utilizing them in developmental studies, disease modeling and transplantation.

KEY WORDS: Human pluripotent stem cells, Retina, Cell culture, Photoreceptors, Differentiation, Organoids

INTRODUCTION

The capacity to generate bona fide fetal-stage neural retinal cell types and tissues from human embryonic and induced pluripotent stem cells (hESCs and hiPSCs; collectively, hPSCs) has spurred their use in disease modeling (Tucker et al., 2011, 2013; Jin et al., 2012; Phillips et al., 2014; Yoshida et al., 2015; Arno et al., 2016; Parfitt et al., 2016; Megaw et al., 2017; Schwarz et al., 2017; Sharma et al., 2017; Shimada et al., 2017; Deng et al., 2018) and photoreceptor (PR) replacement efforts (Lamba et al., 2009, 2010; Hambright et al., 2012; Barnea-Cramer et al., 2016; Shirai et al., 2016; Chao et al., 2017; Gonzalez-Cordero et al., 2017; Mandai et al., 2017; Zhu et al., 2017, 2018; Iraha et al., 2018; Lakowski et al., 2018; McLelland et al., 2018; Gagliardi et al., 2018). Most of these studies employ hPSC differentiation methods that propagate retinal progeny as isolated 3D optic vesicle-like structures (OVs), also known as retinal organoids, in suspension culture (Meyer et al., 2009, 2011; Nakano et al., 2012; Phillips et al., 2012, 2018b; Sridhar et al., 2016; Reichman et al., 2014; Zhong et al., 2014; Kuwahara et al., 2015; Mellough et al., 2015; Singh et al., 2015; Lowe et al., 2016; Wiley et al., 2016; Gonzalez-Cordero et al., 2017; Wahlin et al., 2017; Ovando-Roche et al., 2018; Hallam et al., 2018; Luo et al., 2018). Benefits of these 3D culture techniques include attainment of high percentages of retinal cell types with low or absent non-retinal contamination and a predilection to self-organize into highly mature tissue structures. The latter finding has garnered particular attention, with numerous reports showing segments of isolated retinal organoids with native-appearing laminar organization and cellular ultrastructure (Phillips et al., 2012; 2018b; Zhong et al., 2014; Kuwahara et al., 2015; Lowe et al., 2016; Parfitt et al., 2016; Gonzalez-Cordero et al., 2017; Wahlin et al., 2017; Deng et al., 2018; Lakowski et al., 2018; Hallam et al., 2018; Luo et al., 2018). However, shortcomings have also been evident, such as the presence of ectopic retinal cells and abnormal structures, loss of inner retinal cell types over time, and a relative lack of uniformity within and among organoids (Zhong et al., 2014; Browne et al., 2017; Lowe et al., 2016; Gonzalez-Cordero et al., 2017; Deng et al., 2018; Phillips et al., 2018b; Hallam et al., 2018). In addition, genetic and epigenetic differences exist between non-isogenic hPSC lines, which may introduce further variability into retinal organoid cultures (Nazor et al., 2012; Choi et al., 2015). Although such findings are not surprising in a complex and dynamic culture system, they can impact results and confound data interpretation, and thus necessitate consideration and – if possible – mitigation when embarking on organoid-based studies.

As retinal differentiation in hPSC cultures approximates a human developmental timeline, one common approach to addressing variances in organoid cultures is by simply aligning experimental samples by elapsed differentiation time. Although this method offers some solace to investigators, experience with hPSC-derived retinal pigment epithelium (RPE) has shown that morphological and/or functional indicators are essential to assure comparability between individual cultures (Bharti et al., 2011; Singh et al., 2013; Miyagishima et al., 2016). Unfortunately, for numerous reasons, 3D retinal organoids do not lend themselves to the high level of live

[1]Waisman Center, University of Wisconsin-Madison, Madison, WI 53705, USA. [2]Morgridge Institute for Research, University of Wisconsin-Madison, Madison, WI 53706, USA. [3]Department of Pathology and Laboratory Medicine, University of Wisconsin-Madison, Madison, WI 53705, USA. [4]McPherson Eye Research Institute, University of Wisconsin-Madison, Madison, WI 53705, USA. [5]Aragon Institute for Health Research (IIS Aragón), Lozano Blesa University Hospital, Zaragoza 50009, Spain. [6]Department of Ophthalmology, Lozano Blesa University Hospital, Zaragoza 50009, Spain. [7]Murdoch Children's Research Institute, The Royal Children's Hospital, Parkville, Victoria 3052, Australia. [8]Department of Paediatrics, University of Melbourne, Parkville, Victoria 3052, Australia. [9]Department of Ophthalmology, Wilmer Eye Institute, Johns Hopkins University School of Medicine, Baltimore, MD 21287, USA. [10]Department of Biomedical Engineering, University of Wisconsin-Madison, Madison, WI 53706, USA. [11]Department of Ophthamology and Visual Sciences, University of Wisconsin-Madison, Madison, WI 53705, USA.

*Author for correspondence (dgamm@wisc.edu)

J.S., 0000-0002-4502-6402; Z.E., 0000-0003-3154-4281; V.M.S., 0000-0003-3318-7986; D.M.G., 0000-0002-8152-613X

Received 7 September 2018; Accepted 10 December 2018

Development (2019) 146, dev171686. doi:10.1242/dev.171686

scrutiny afforded by purified monolayer cultures of hPSC-RPE. As such, efforts to determine comparability across organoid cultures are usually limited to qualitative post-fixation analyses of selected areas within sections, which reveal only a minute fraction of the features present in a single organoid, much less an entire culture population.

To gain a better understanding of the consistency and behavior of 3D retinal organoid cultures, we differentiated 16 hPSC lines (hESC and hiPSC, including isogenic and non-isogenic lines) using an established protocol (Meyer et al., 2011) with adaptations from other frequently referenced reports that reliably improved organoid yield and organization (Zhong et al., 2014; Kuwahara et al., 2015). The resulting hybrid method yielded starting organoid cultures that were broadly indistinguishable across hPSC lines and differentiations. Observation of each of these cultures for at least 175 days revealed three stages of retinal organoid development that could be easily discerned morphologically by light microscopy (LM) and optical coherence tomography (OCT) in live cultures. Subsequent immunocytochemical (ICC) analyses showed that stage 1 organoids contained neural retina progenitors (NRPCs) within a developing outer neuroblastic layer, along with numerous retinal ganglion cells (RGCs) and rare starburst amacrine cells (SACs) that formed an inner RGC layer as well as a rudimentary, discontinuous inner plexiform-like layer (IPL). Stage 2 represented a transition period during which the discrete RGC layer gradually deteriorated and NRPCs underwent progressive differentiation into PRs, horizontal cells (HCs) and amacrine cells (ACs). Stage 3 was marked by formation of PR outer segments and other features of advanced outer retinal organization, along with continued loss and/or disorganization of inner retinal cell types and layers. 3D fluorescence reconstruction imaging allowed further evaluation of stage 3 organoid structure and PR subtype distribution in a broader context. Also prominent by stage 3 were Müller glia (MG), the surface-directed processes of which contributed to the outer structural framework of organoids, including formation of an external limiting membrane at the base of PR inner segments. In contrast, inward-projecting MG processes appeared disorganized, occupying much of the core of stage 3 organoids.

Together, these findings set forth a practical means to sort and compare like-staged retinal organoids in live cultures that takes into account parameters beyond time spent in culture. Although further refinements in 3D retinal culture methods will undoubtedly occur that may affect organoid structure and behavior, the added use of non-temporal evaluation criteria should enhance rigor and reproducibility of future retinal organoid studies regardless of differentiation protocol.

RESULTS

LM identification of three distinct morphological stages of hPSC-derived retinal organoid development

To search for common, distinguishing features of differentiating retinal organoids, we used LM to examine live cultures derived from a diverse cohort of 16 hPSC lines differentiated for at least 175 days *in vitro* (Table 1). The hPSC lines, which were independently cultured and differentiated by up to 12 different laboratory personnel over the course of 3 years, included four hESC lines (three of which had undergone gene editing) and 12 hiPSC lines (four normal controls, five from patients with retinal degenerative diseases, and three that underwent gene editing). Although 3D retinal differentiation protocols vary, most incorporate an early step that generates OVs containing an enriched starting population of NRPCs, which provides a common starting point regardless of method. For this study, we combined elements of three frequently referenced protocols that together generate consistently high yields of hPSC-OVs with excellent long-term survival (up to 470 days, the longest time point tested). In addition, we strove to minimize media cost and complexity wherever possible. This hybrid 3D protocol (Fig. 1A) evolved from a technique initially described by Meyer et al. (2011) and modified by Zhong et al. (2014) to promote prolonged maintenance of retinal laminar structure. More recently, Kuwahara et al. (2015) reported improvement in OV production with brief, early exposure of hESC cultures to BMP4. To test the reproducibility of this finding across multiple lines, we treated seven hiPSC lines with or without a single dose of BMP4 at day 6 of differentiation, followed by one-half media changes every 3 days until day 16, and noted a 6.0±1.6-fold increase in OV production per 6-well starter plate (Fig. S1A). In addition, we observed a more-defined OV colony appearance in BMP4-treated cultures after plating, which facilitated their identification, dissection, and transfer into suspension cultures at day 30 (Fig. S1B). These findings prompted us to incorporate a single, early BMP4 pulse in our base differentiation protocol.

We then monitored all hPSC-OV suspension cultures (herein referred to as organoids) for at least 175 days (range=175-470 days) and took note of their LM appearance over time. All organoids initially possessed a continuous, or nearly continuous, phase-bright outer neuroepithelial rim (Fig. 1C). This well-defined morphology,

Table 1. Cell line description

Line	Type	Gender	Derivation	Cell source	Description
1096	hiPSC	M	CDI MyCell	Blood	Retinitis pigmentosa
1013	hiPSC	M	CDI MyCell	Blood	Normal
1579	hiPSC	F	CDI MyCell	Blood	Leber's congenital amaurosis
1580	hiPSC	F	CDI MyCell	Blood	Leber's congenital amaurosis
1581	hiPSC	M	CDI MyCell	Blood	Normal
1582	hiPSC	M	CDI MyCell	Blood	Normal
591	hiPSC	M	CDI MyCell	Blood	Usher syndrome
595	hiPSC	M	CDI MyCell	Blood	Usher syndrome
597	hiPSC	F	CDI MyCell	Blood	Normal
Clone 7	hiPSC	M	Howden et al., 2015	Fibroblast	Gene edited
Clone 31	hiPSC	M	Howden et al., 2015	Fibroblast	Gene edited
Clone J	hiPSC	M	Howden et al., 2015	Fibroblast	Gene edited
WA09	hESC	F	WiCell	WA09	Normal
CRX$^{+/tdTomato}$	hESC	F	Phillips et al., 2018a	WA09	PR reporter line
BRN3B reporter	hESC	F	Sluch et al., 2017	WA07	RGC reporter line
NRL$^{+/eGFP}$	hESC	F	Phillips et al., 2018b	WA09	Rod reporter line

Development (2019) 146, dev171686. doi:10.1242/dev.171686

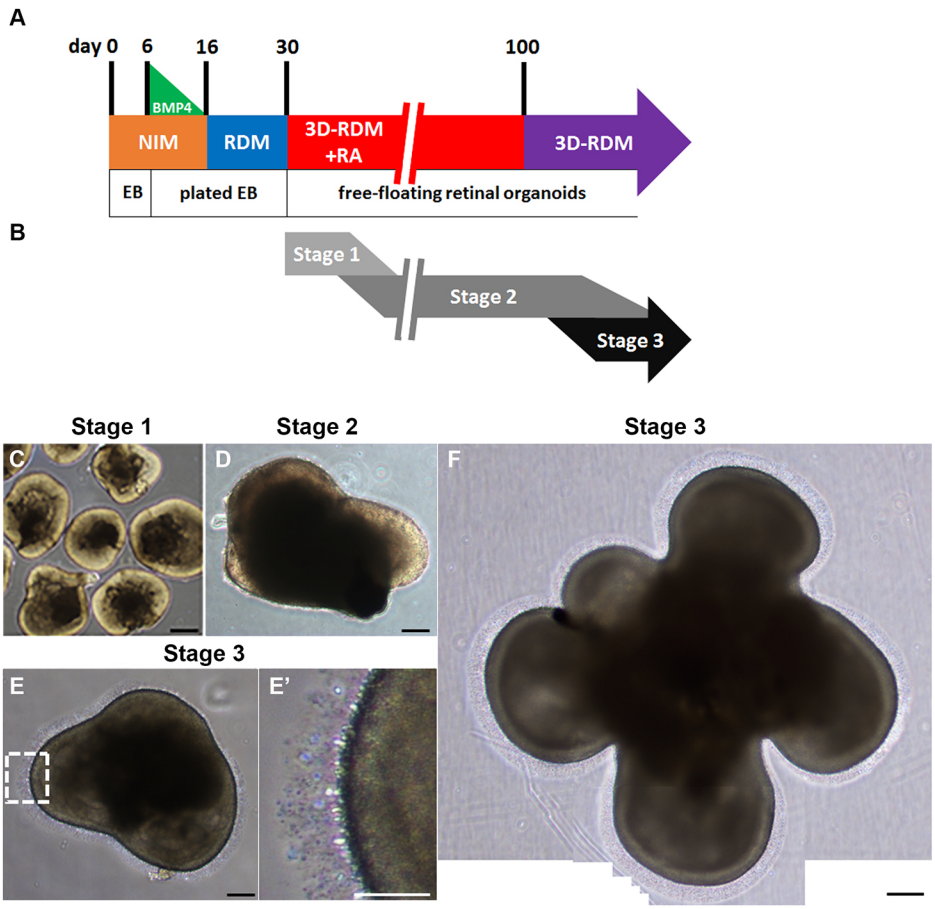

Fig. 1. Light microscopic identification of distinct morphological stages in live cultures of differentiating hPSC-derived 3D retinal organoids. (A) Schematic of the hybrid hPSC retinal differentiation protocol used for this study. (B) Timing and overlap of morphological stages observed across all 16 lines tested. (C-F) Representative live LM phase images of stage 1 (C), stage 2 (D) and stage 3 (E,F) organoids. E′ is a magnification of the boxed area in E showing hair-like surface projections, and F shows a multi-lobulated stage 3 organoid created through the spontaneous fusion of multiple co-cultured organoids. Scale bars: 100 µm (C-E,F); 50 µm (E′).

which we designated stage 1, was maintained for up to 6 weeks in organoid culture (Fig. 1B). Organoids increased in size during this period and eventually developed a phase-dark core with a reduced or absent phase-bright outer rim, at which point they were labeled morphological stage 2 (Fig. 1D). Stage 2 organoids grown in bulk cultures often merged together and adopted a lobular appearance with one or more localized regions of RPE (Fig. S1C), but invagination of organoids with direct apposition of pigmented and non-pigmented layers (as occurs during true optic cup formation) was never observed. Stage 2 organoids arose as early as 3-4 weeks after isolation, and some persisted in this morphological stage. However, the majority transitioned between 17-24 weeks post-isolation to a third stage marked by the distinct appearance of hair-like surface appendages (Fig. 1E,F). This final stage extended indefinitely and was further defined by re-emergence of a thin outer rim structure. Importantly, substantial temporal overlap of stage 1 and 2 organoids, as well as stage 2 and 3 organoids, was commonly observed in individual cultures (Fig. 1B, Fig. S1D), although progression through all three stages occurred invariably in every line (Fig. S2). Together, these findings suggest that LM morphological criteria could be a useful and perhaps necessary adjunct for sorting and comparing live retinal organoids within and across cultures and hPSC lines.

3D morphological analysis of staged retinal organoids using OCT

To correlate LM appearance with 3D structure, we sorted organoids by stage and subjected them to OCT, which provides unbiased insight into internal anatomy as well as overall form and surface topography. Of note, Browne et al. (2017) previously established OCT as a method for assessing 3D cultured retinal organoids. OCT revealed an open bowl-like contour for stage 1 organoids (Fig. 2A-C, Movie 1) and an enclosed spheroidal shape with a hollow core for stage 2 organoids (Fig. 2D-F, Movie 2). Both stage 1 and stage 2 organoids had a uniform tissue reflectance with little or no detectable internal structure except for the optically clear center at stage 2. OCT of stage 3 organoids revealed more complex structural elements, including the aforementioned hair-like surface appendages, as well as alternating high and low reflectance layers near the outer rim (Fig. 2G-I, Movie 3). Interestingly, stage 3 organoids did not possess a hollow core like their stage 2 predecessors. Thin sections of stage 1, 2 and 3 organoids confirmed the differences in cellular stratification and interior structure inferred by OCT (Fig. 2J-L). More specifically, stage 1 and 2 organoids possessed little discernable laminar structure in contrast to stage 3, and stage 2 organoids were unique in possessing a sequestered central region devoid of both cells and matrix. Overall, OCT not only reinforced the distinct morphologies noted by LM, but also uncovered additional anatomical features that further distinguished organoids from each of the three stages.

Stage 1 encompasses a period of NRPC proliferation and production of a robust RGC layer harboring SACs

To determine the identity and distribution of retinal cell types in stage 1 retinal organoids, we performed ICC using markers of early retinogenesis, including VSX2 and Ki67 (MKI67; NRPCs and proliferating cells, respectively), SNCG (RGCs), CaR (calretinin, also known as calbindin 2; RGCs and ACs) and CHAT (SACs). Prior reports have shown consistently that early 3D retinal organoids contain NRPCs that give rise initially to RGCs (Meyer et al., 2011; Phillips et al., 2012, 2014, 2018b; Nakano et al., 2012; Reichman

Development (2019) 146, dev171686. doi:10.1242/dev.171686

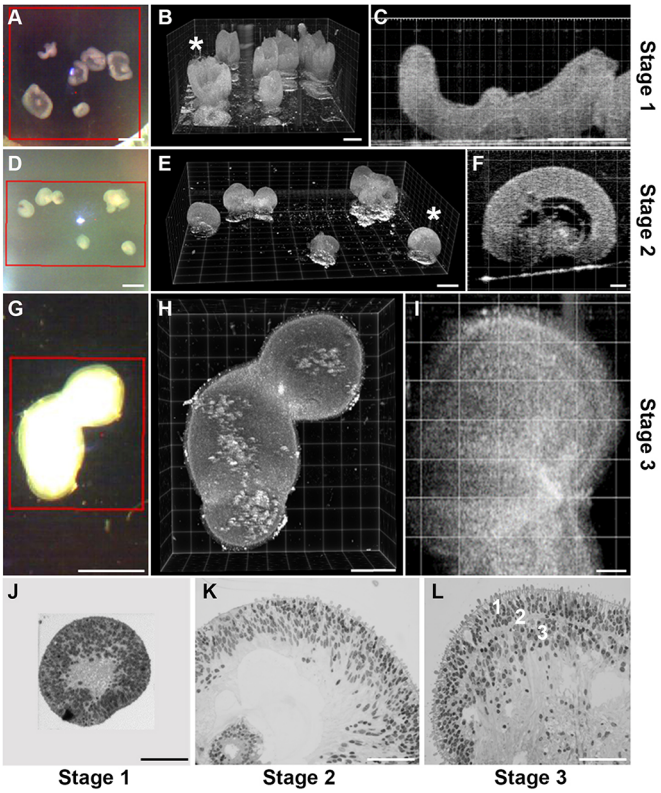

Fig. 2. OCT analysis of morphologically staged retinal organoids. (A-C) Stage 1 organoids (d35): LM image (A), 3D OCT rendering (B) and magnified OCT slice (C) of an organoid (marked with an asterisk in B) showing the cup-like shape characteristic of stage 1 organoids. (D-F) Stage 2 organoids (d54): LM image (D), 3D OCT rendering (E) and magnified OCT slice (F) of an organoid (marked with an asterisk in E) showing the thick outer rim and hollow center characteristic of stage 2 organoids. (G-I) Stage 3 organoid (d250): LM image (G), 3D OCT rendering (H) and magnified OCT slice (I) of the organoid showing hair-like surface projections, thin outer rim, and alternating high and low reflectance lamina. (J-L) Brightfield images of thin sections of staged organoids showing the homogenous outer rim of a stage 1 organoid (J), the relatively homogenous outer rim and hollow center of a stage 2 organoid (K), and three distinct cellular or acellular lamina (labeled 1, 2, 3) and matrix-filled core of a stage 3 organoid (L). Scale bars: 1 mm (A,D,G); 500 µm (B,C,E,H); 100 µm (F,I); 50 µm (J-L).

et al., 2014; Zhong et al., 2014; Singh et al., 2015; Lowe et al., 2016; Wiley et al., 2016; Hallam et al., 2018). Isolated stage 1 organoids confirmed this finding across all hPSC lines and cultures, with an abundance of RGCs lining the inner aspect of organoids beneath an overlying population of VSX2$^+$ NRPCs (Fig. 3A-E, Fig. S3A-J). Ki67 immunostaining was concentrated within NRPC nuclei along the outer organoid rim, corresponding to the apical location where NRPC division occurs during interkinetic nuclear migration (Fig. 3B) (Baye and Link, 2007). Interestingly, we also noted discontinuous gaps in nuclear immunostaining between the RGC and NRPC layers, reminiscent of an early IPL. As such, we also looked for the presence of SACs, an early-born subtype of AC that helps define inner retinal structure, including formation of the IPL (Famigletti, 1983; Rodieck and Marshak, 1992). CHAT immunostaining, which is specific for SACs in the retina, revealed their rare presence within both the RGC layer and the discontinuous IPL-like regions (Fig. 3F-J, Fig. S3K-O). Therefore, stage 1 is marked by (1) expansion of NRPCs within an outer neuroblastic layer and (2) early but incomplete definition of the innermost retinal layers.

Stage 2 represents an intermediate developmental phase highlighted by differentiation of PR and retinal interneuron populations

ICC of early stage 2 organoids revealed OC1 (ONECUT1)$^+$ and CaR$^+$ cells interspersed among RGCs within the inner aspect of organoids, which likely represent HCs and ACs, respectively, based on their location and timing of expression (Fig. 4A-D, Fig. S4A-H). Also at early stage 2, some RGC processes ectopically extended to the organoid surface, passing through a developing outer mantle of OTX2$^+$ PR precursors (Fig. 4E-H, Fig. S4I-P). Additional ICC analysis using primary antibodies directed against CRX and RCVRN confirmed the PR identity of many outer retinal cells (Fig. 4I-L, Fig. S5A-H). Furthermore, PRs at or near the organoid surface assumed a radial orientation and often expressed markers of early cone (ARR3) or rod (NRL) commitment, although cone and rod marker expression was also seen deeper within organoids (Fig. 4I-P, Fig. S5I-L). However, despite the emerging cellular complexity and broad tissue-like organization of stage 2 organoids, clear separation of nuclear and plexiform layers was infrequently observed at this stage (Fig. 4A,E,I,M).

Stage 3 specifies the presence of mature outer nuclear and plexiform layers with metabolically active PRs that form specialized ribbon synapses

A one-cell-thick layer of cones expressing ARR3 and either M/L- or S-opsin was located along the outermost surface of stage 3 organoids, with an underlying multiple-cell-thick layer of NRL$^+$ and NR2E3$^+$ rod nuclei (Fig. 5A-C″). The overall ratio of rods to cones in stage 3 organoids was 4:1 (Fig. 5D,E), and within the cone subpopulation,

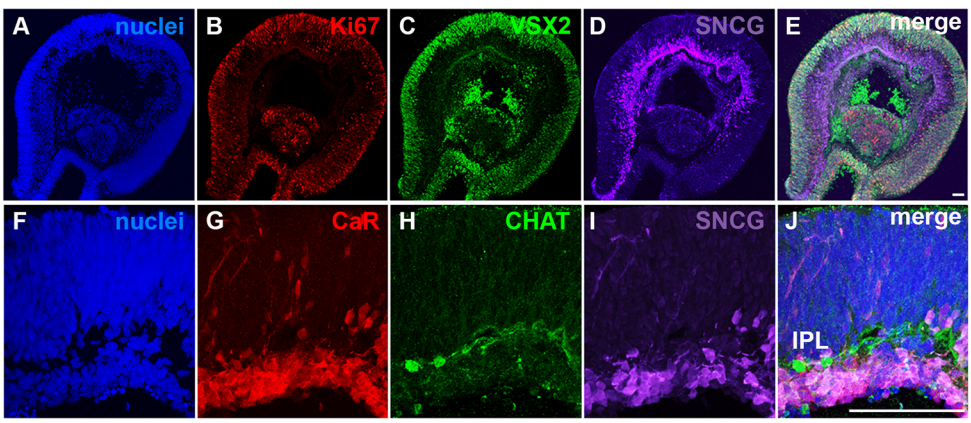

Fig. 3. Stage 1 organoids comprise proliferative NRPCs, RGCs and rare SACs. (A-E) ICC analysis of a representative stage 1 organoid (d35) revealing the presence of Ki67$^+$/VSX2$^+$ proliferative NRPCs (A-C; merge in E) overlying an internal layer of SNCG$^+$ RGCs (D; merge in E). (F-J) Magnified ICC images of a stage 1 organoid (d35) showing the presence of CaR$^+$ cells (indicative of ACs and RGCs), SNCG$^+$ RGCs and CHAT$^+$ SACs (F-I; merge in J) with processes forming a rudimentary IPL. Scale bars: 100 µm.

Development (2019) 146, dev171686. doi:10.1242/dev.171686

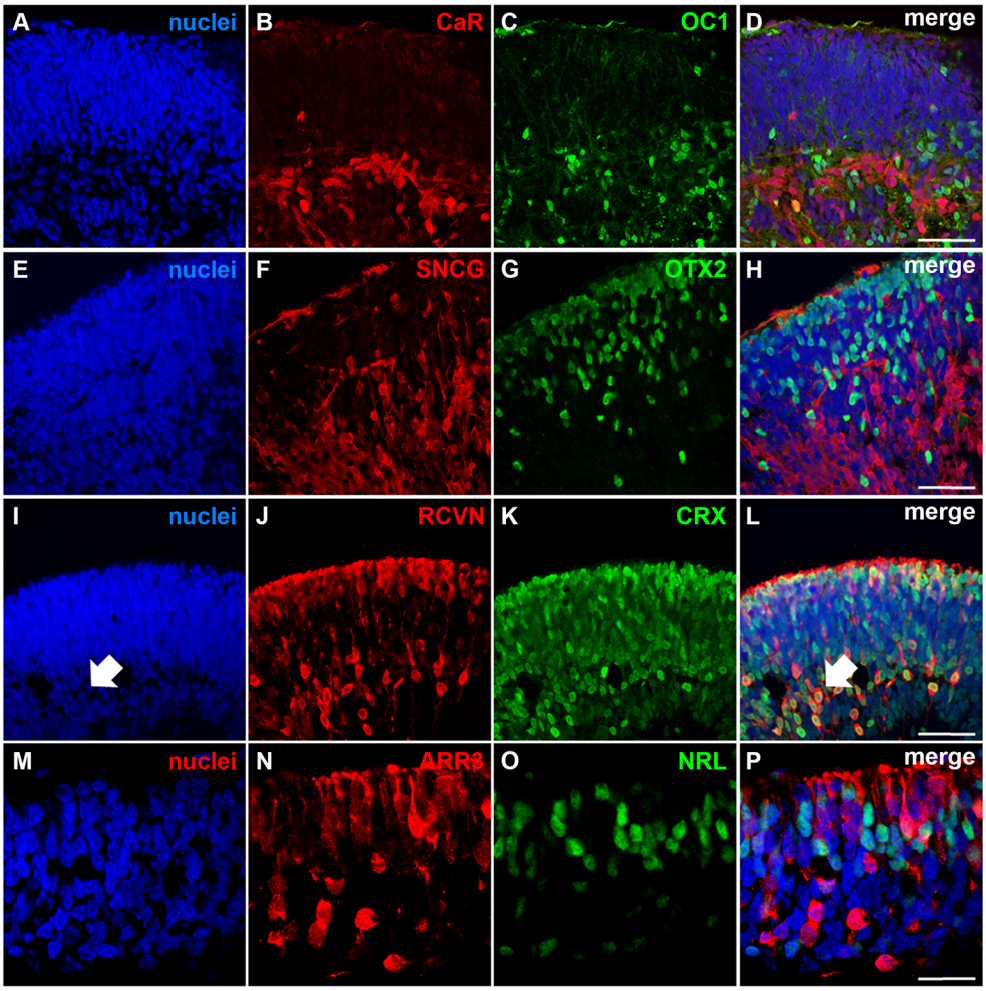

Fig. 4. Stage 2 organoids contain abundant PR precursors and maturing cones and rods, as well as RGCs, HCs and ACs. (A-D) ICC images of a representative stage 2 organoid (d80) showing CaR$^+$ cells (ACs and RGCs) (B) and OC1$^+$ HC progenitors (C; merge in D). (E-H) ICC images of a representative stage 2 organoid (d80) comparing expression of SNCG$^+$ RGCs (F) and early OTX2$^+$ PR progenitors (G; merge in H) along the inner and outer aspects of the organoid mantle, respectively. (I-L) ICC images of a representative stage 2 organoid (d80) revealing an abundance of maturing CRX$^+$/RCVRN$^+$ PRs (J,K; merge in L) predominantly within the cell-dense, outer aspect of the organoid, along with some PRs located deep to this region (arrow in I and L). (M-P) ICC images of an older stage 2 organoid (d140) revealing differentiating ARR3$^+$ cones and NRL$^+$ rods. Scale bars: 50 µm.

M/L-cones outnumbered S-cones 8:1 (Fig. 5F,G). Interestingly, unlike M/L-cone opsin immunostaining, rod opsin immunostaining was often non-uniform across the surface of organoids (Fig. 5H-L, Fig. S6, Movies 4 and 5), likely indicative of the later and more extended window of rod versus cone development. Overall, the structural and numerical distribution of PR subtypes in the stage 3 organoid outer nuclear layer (ONL) most closely resembles that of the human perifoveal retina, as more-peripheral ONL regions display higher rod:cone ratios whereas the central fovea is M/L-cone exclusive (Osterberg, 1935; Yanoff and Duker, 2013).

The hair-like surface appendages that herald stage 3 morphology have been shown previously to represent developing PR outer segments (OSs) (Zhong et al., 2014; Lowe et al., 2016; Gonzalez-Cordero et al., 2017; Wahlin et al., 2017; Phillips et al., 2018b). We confirmed this finding with immunostaining for M/L-opsin, ARL13b and pericentrin (PCN; PCNT), as well as with transmission electron microscopy (TEM) (Fig. 6A-F, Fig. S7A-E′). Rod and cone OSs were maintained for up to 470 days, the latest time point assayed (Fig. 6G-J). TEM specifically revealed the presence of fetal-stage OS structures containing unstacked disks attached via connecting cilia to mitochondria-rich inner segments (ISs) (Fig. 6B,K,L, Fig. S7D-E′). To gain further insight into the IS and OS structures of stage 3 PRs, we performed dynamic optical metabolic imaging (OMI) to measure the autofluorescence (AF) signatures of NAD(P)H and retinol/retinoic acid. We found that NAD(P)H AF was localized to the thin region containing PR ISs, whereas retinol/retinoic acid AF was present in elongated OSs within the outer retina as well as more diffusely in the inner retina corresponding to the location of ectopic PRs (see below) (Fig. 6M; LM image of stage 3 organoid and OMI on an additional line in Fig. S7F-H). These results extend findings obtained using younger organoids that did not contain clear ISs or OSs (Browne et al., 2017). Altogether, OMI suggests that PRs within stage 3 retinal organoids are metabolically active cells equipped for light detection, which is consistent with their functional demands and purpose *in vivo*.

Deep relative to the ONL was a thin nuclei-free layer (Fig. 7A,I,M), the position of which corresponded to the outer plexiform layer (OPL) of the retina, a structure that contains the specialized ribbon synapses that couple PRs of the ONL with bipolar and horizontal cells of the inner nuclear layer (INL). Indeed, expression of PR pre-synaptic markers, such as VGLUT1 (SLC17A7) and CTBP2, was concentrated in this layer within stage 3 organoids (Fig. 7A-E, Movie 6). Importantly, cones demonstrated broad axon terminals (pedicles; Fig. 7F) as opposed to the compact terminals characteristic of rods (spherules; Fig. 7G; also see Movie 7). Further evidence of synaptic connectivity between PR axon terminals and cells of the INL was found by TEM, which showed the presence of vesicle-laden ribbon synapses surrounding invaginated dendritic terminals (Fig. 7H, Fig. S8A-B′). A discontinuous INL containing bipolar cells (BPCs) was also present at stage 3, as determined by expression of VSX2 (which marks nuclei of BPCs at this stage of retinogenesis), PKCα (rod BPCs) and/or Gαo (GNAO1; rod and cone ON BPCs). (Of note, the

Development (2019) 146, dev171686. doi:10.1242/dev.171686

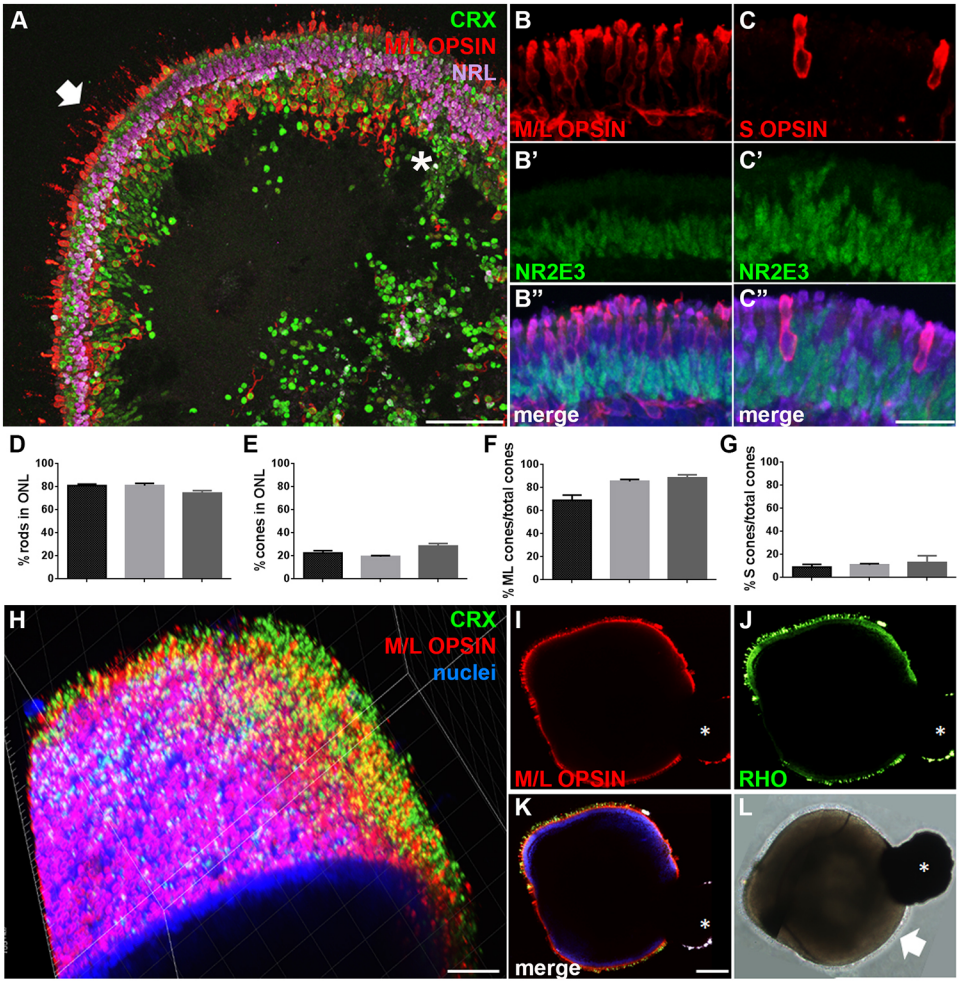

Fig. 5. Stage 3 organoids possess a well-defined ONL-like layer with maturing rods and cones. (A) ICC image of a representative stage 3 organoid (d200) demonstrates an ONL region containing an outermost layer of M/L-opsin$^+$/CRX$^+$ cones with M/L-opsin$^+$ surface projections (arrow), and an underlying three- to five-nuclei-thick layer of NRL$^+$/CRX$^+$ rods. Mislocalized CRX$^+$ PRs, some co-expressing M/L-opsin or NRL, are also present below the ONL (asterisk). (B-C″) Higher magnification ICC images of representative stage 3 organoids (d160) showing the location and morphology of M/L-opsin$^+$ (B) and S-opsin$^+$ (C) cones and NR2E3$^+$ rods in the ONL (B′,C′, merge in B″,C″). (D,E) Percentage of NRL$^+$ rod (D) and ARR3$^+$ cones (E) within the ONL of stage 3 organoids derived from three different WT hiPSC lines (minimum of six organoids/line; mean±s.e.m. is plotted). (F,G) Percentages of M/L-opsin$^+$ (F) and S-opsin$^+$ (G) cones within the total ARR3$^+$ cone population. (H) 3D multiphoton rendering of a d250 stage 3 organoid showing the surface distribution of RHO$^+$ rods and M/L-opsin$^+$ cones (see also Movie 4). (I-K) Confocal images of a single *z*-plane through the organoid shown in H immunostained for M/L-opsin (I) and RHO (J; merge in K). (L) LM image of the organoid taken prior to fixation showing a lobulated region of pigmented RPE (asterisk in I-L) and hair-like projections (arrow) covering the remainder of the organoid surface. Scale bars: 100 µm (A,H); 25 µm (B-C″); 500 µm (I-L).

presence of G0α$^+$/PKCα$^-$ cells provides the first definitive identification of ON cone BPCs in hPSC-derived retinal cultures.) (Fig. 7I-P, Fig. S8C-G′, Movie 7).

In summary, across all hPSC lines and differentiations tested, the distinct appearance of stage 3 organoids by LM was unequivocally indicative of a highly developed ONL and OPL, as well as the presence of a less uniform INL containing BPCs and other retinal interneurons (Table 2).

Inner regions of stage 3 retinal organoids display structural disorganization, loss and displacement of RGCs and SACs, and ectopic differentiation of PRs

Compared with the remarkably native-appearing outer layers of stage 3 organoids, deeper regions (i.e. cells and processes located internal to the OPL) demonstrated a cellular composition that less reliably approximated normal retina. Disorganization and cell loss generally worsened as a function of depth beyond the OPL, culminating in the substantial deterioration and mislocalization of the formerly abundant RGCs that lined the interior of stage 1 organoids (Figs 3 and 4). To follow RGC fate across all three stages in more detail, we employed a *BRN3b*-P2A-tdTomato-P2A-*Thy1.2* RGC reporter hESC line developed by Don Zack's lab (Sluch et al., 2017) that fully labels RGC cytoplasm including their processes (Fig. 8). In stage 1 and early stage 2 organoids, numerous RGCs were present in a discrete interior ganglion cell layer (GCL), with processes that extended inward toward the organoid core as well as outward through the neuroblastic layer where they often covered the organoid surface as noted above (Fig. 4H, Fig. 8A-D). At later times, *BRN3b*-tdTomato$^+$ RGC processes ceased to be present on the organoid surface, owing either to retraction or to cell death (Fig. 8E-P). By stage 3, remaining RGCs were sparse and disorganized with haphazard, blunted processes (Fig. 8M-P). Concomitant with the decline in the GCL was an increase in the number of ectopic PR lineage cells found within the interior of aging organoids (Fig. 8C,G,K,O), which, despite their misplacement, underwent progressive maturation similar to PRs located in the organoid ONL (Fig. 7J, Movie 7). This progressive loss of RGCs and sub-OPL disorganization was observed in all hPSC lines (Table 2, Fig. S9A-H) along with a similar loss of SACs (Fig. S9I-P). Thus, in contrast to their outer strata, stage 3 organoids often lacked internal organization and underwent a shift in cellular constituency with progressive loss of RGCs and gain of ectopic PRs.

MG are abundant in stage 3 retinal organoids where they contribute to formation of an outer (but not inner) limiting membrane

Lastly, we examined whether MG, one of the last neural retina cell types generated from NRPCs, were present within the INL of stage 3 retinal organoids. Immunostaining for CRALBP (RLBP1) localized MG cell bodies to the INL and also demonstrated extension of MG processes through the OPL and ONL, terminating at the junction between the PR inner and outer segments (Fig. 9A-F). At the IS/OS junction, the MG end feet formed a thin, continuous structure

Development (2019) 146, dev171686. doi:10.1242/dev.171686

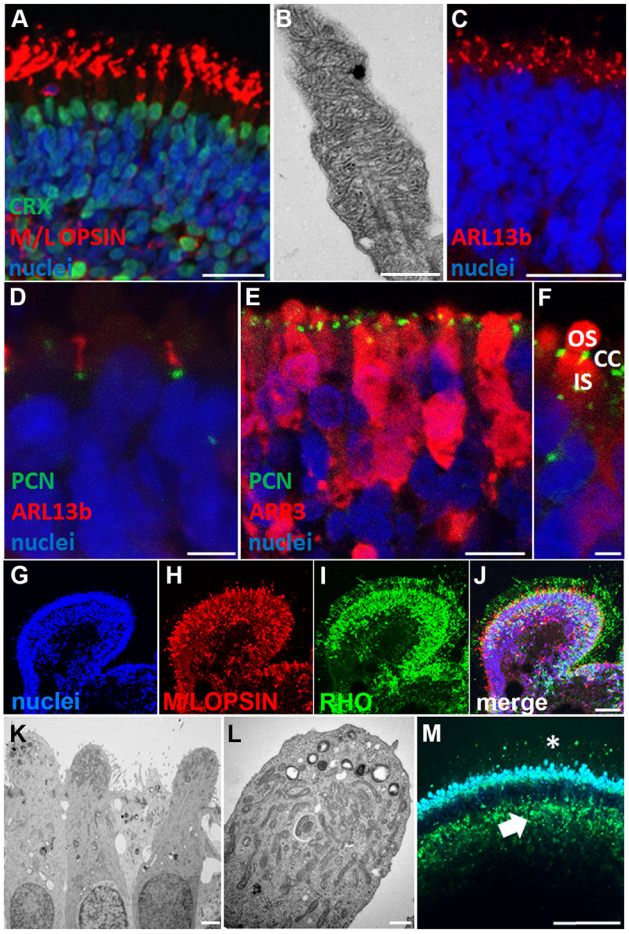

Fig. 6. PRs in stage 3 organoids demonstrate maturing outer segments and metabolically active inner segments. (A) Representative high magnification ICC image of a stage 3 organoid (d160) showing the location and morphology of M/L-opsin$^+$ cone outer segments relative to CRX$^+$ PR nuclei. (B) Electron micrograph of an outer segment from a d225 stage 3 organoid showing partially stacked discs. (C) ICC of a d240 stage 3 organoid showing ARL13b$^+$ outer segments. (D) Immunostaining for outer segment cilia (ARL13b) and basal bodies (PCN) in a d200 stage 3 organoid. (E,F) Stage 3 (d160) organoid co-immunostained for PCN and cone ARR3. CC, connecting cilium. (G-J) ICC of a d470 stage 3 organoid showing persistent and elongated M/L-opsin$^+$ cone (H) and RHO$^+$ rod (I; merged in J) outer segments. (K,L) Electron micrographs of mitochondria-rich inner segments of stage 3 organoids. (M) Autofluorescence intensity image of a d250 stage 3 organoid showing metabolically active, NADP(H)-rich inner segments (blue) and retinol-containing regions (green) corresponding to outer segments (asterisk) and mislocalized PRs within the inner retinal layer (arrow). Scale bars: 25 µm (A,C); 400 nm (B); 2 µm (D,F,K); 5 µm (E); 50 µm (G-J); 600 nm (L); 100 µm (M).

strongly reminiscent of the outer limiting membrane (OLM) (Fig. 9G-I). The OLM acts *in vivo* as a key barrier to migration of foreign material into the neural retina from the subretinal space and also contributes to the maintenance of outer retinal structure. MG processes also extended inward in a profuse and disorganized fashion, occupying much of the sparsely nucleated core of stage 3 organoids (Fig. 9A-C). The sustained presence of MG in stage 3 retinal organoids is of significant note given their importance in the formation and maintenance of normal neural retina anatomy and in PR (particularly cone) function and homeostasis. Perhaps equally important to note is the absence of a discrete inner limiting membrane (ILM), which is also formed by MG *in vivo* in concert with retinal astrocytes, the latter of which are not generated by NRPCs and thus are not inherently present in organoids. The contrast in outer versus inner organization of stage 3 MG processes conspicuously parallels the general dichotomy of outer versus inner cellular stratification observed in these organoids, suggesting an important but incompletely tapped role for MG and the ILM in hPSC retinal organoid development.

DISCUSSION

Methods to generate 3D retinal cultures from hPSCs have increased in number substantially since their first descriptions (Meyer et al., 2011; Nakano et al., 2012; Phillips et al., 2012, 2018b; Sridhar et al., 2016; Reichman et al., 2014; Zhong et al., 2014; Kuwahara et al., 2015; Mellough et al., 2015; Singh et al., 2015; Lowe et al., 2016; Wiley et al., 2016; Gonzalez-Cordero et al., 2017; Wahlin et al., 2017; Ovando-Roche et al., 2018; Hallam et al., 2018; Luo et al., 2018). Even so, most protocols follow a common developmental sequence and time frame that closely mimic normal human retinogenesis, including production of a starting population of OVs that display a phase-bright, palisading neuroepithelial rim. This obedience to highly conserved developmental principles offers reassurance of the ultimate authenticity of the cells produced from the resulting retinal organoids. Indeed, the striking similarities among culture protocols suggest an overall robustness of the intrinsic hPSC neural retina differentiation process. However, many features of differentiating and mature 3D hPSC retina cultures – particularly those grown in isolation without forebrain or other non-retinal tissue components – are not reflective of normal development and/or can vary considerably within and between organoids. Such inconsistencies have been sporadically reported (Browne et al., 2017; Deng et al., 2018; Phillips et al., 2018b), but are not always evident in sections that focus on an isolated region of a single organoid. These acknowledged but largely unexplored limitations of 3D hPSC culture systems were the impetus for the recent '3D Retinal Organoid Challenge 2020' sponsored by the National Eye Institute.

Building on our long-term experience with purified 3D retinal organoids, we sought to (1) search for a facile means to developmentally stage live organoids and improve quality control of these systems, and (2) describe the recurring strengths and limitations of organoid cultures at each stage. Given that the initial hPSC-OV population can be readily excised and/or sorted from non-OVs by LM features, we suspected that LM also would be useful later in the differentiation process to pool organoids of like composition and structure. Presently, time in culture is the sole criterion used to group organoids for comparative analyses, a practice that is inadequate for most other dynamic culture systems, including hPSC-RPE.

To assure reproducibility, we required that live-staging features be invariant across 16 hPSC lines and independent of changes in passage number, reagent lots, or user experience. We also settled upon a single differentiation protocol that incorporated advances described by multiple laboratories that consistently improved OV production and survival. Although variations in methods can influence culture behavior, confidence in the general applicability of our staging system is bolstered by the remarkably common attributes of isolated retinal organoids generated under diverse conditions by numerous labs.

Over the prolonged course of our study, we observed three consistent LM stages in all organoid cultures (Fig. 10). Physical findings used to distinguish stages by LM were confirmed by OCT in live cultures and further analyzed using ICC, TEM and OMI (Table 2). Although broad and overlapping, these LM stages hold

Development (2019) 146, dev171686. doi:10.1242/dev.171686

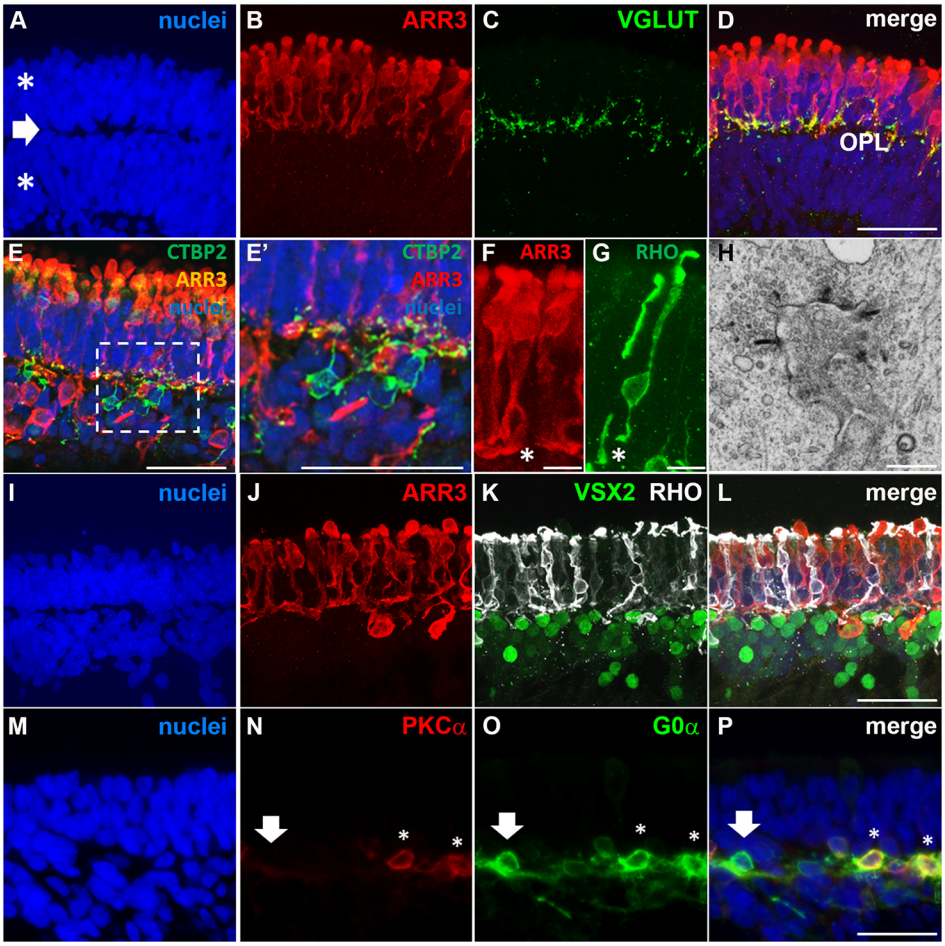

Fig. 7. Stage 3 organoids possess an OPL-like layer, ribbon synapses, and an INL containing rod and cone BPCs. (A-D) ICC images of a stage 3 organoid (d220) showing two distinct nuclear layers (asterisks) separated by a thin nuclei-free zone (arrow) (A). Expression of ARR3 in cone pedicles (B) overlaps with expression of the PR synapse marker VGLUT (C; merge in D) in the OPL. (E,E′) Immunostaining in a d225 stage 3 organoid for the ribbon synapse marker CTBP2 (also known as RIBEYE), which colocalizes with ARR3$^+$ cone pedicles in the OPL. E′ is a magnified image of the boxed region in E. (F,G) ICC of ARR3$^+$ cones and RHO$^+$ rods demonstrating pedicle and spherule morphology, respectively (asterisks). (H) Electron micrograph demonstrating ribbon synapses in a d212 stage 3 organoid. (I-L) ICC images of a d225 stage 3 organoid showing ARR3$^+$ cones (J) and RHO$^+$ rods (K) in the ONL and VSX2$^+$ BPCs in the INL (K; merge in L). (M-P) ICC images demonstrating the presence of PKCα$^+$ rod BPCs (N) and G0α$^+$ ON BPCs (O; merge in P) in a d160 stage 3 organoid. A G0α$^+$/PKCα$^-$ cone ON BPC is indicated with an arrow in N-P and asterisks mark rod BPCs. Scale bars: 50 µm (A-E′,I-P); 10 µm (F,G); 500 nm (H).

practical importance when designing, conducting and interpreting experiments involving hPSC-derived retinal organoids. For example, studies targeting RGCs are best performed at stage 1 or early stage 2 when they are relatively abundant and their processes project to the surface, which facilitates axonal outgrowth after attachment of the RGCs to substrate (Yang et al., 2017; Kobayashi et al., 2018; Langer et al., 2018). The cause of the deterioration and disorganization of RGCs at later stages is not completely clear, but, among other factors, it could be due to an absence of post-synaptic forebrain targets, lack of inner retinal structure, and/or insufficient metabolic support. The persistence of scattered RGCs within stage 3 organoids suggests that mechanism(s) do exist to support long-term RGC health, perhaps mediated by the MG processes that surround them at this stage. Insight into such mechanisms could lead to improved RGC survival and overall inner retinal development.

Table 2. Summary of physical findings for staged organoids

Line	GC d90	GC >d160	INL	Ribbon synapse	ONL/OS
1096	+++	+/–	+	+	+
1013	+++	+/–	+	+	+
1579	+++	+/–	+	+	+
1580	+++	+/–	+	+	+
1581	+++	+/–	+	+	+
1582	+++	+/–	+	+	+
591	+++	+/–	+	+	+
595	+++	+/–	+	+	+
597	+++	+/–	+	+	+
Clone 7	+++	+/–	+	+	+
Clone 31	+++	+/–	+	+	+
Clone J	N	+/–	+	+	+
WA09	+++	+/–	+	+	+
CRX$^{+/tdTomato}$	+++	+/–	+	+	+
BRN3B reporter	+++	+/–	+	+	+
NRL$^{+/eGFP}$	+++	+/–	+	+	+

GC, ganglion cell; N, not tested.

Stage 2 represents a highly dynamic period of organoid development with regard to cell composition, maturation and organization. In particular, PR precursors and subtypes arise and begin to form a discrete ONL, accompanied by generation of BPCs and other retinal interneurons of the INL. Although the changing cellular landscape of stage 2 organoids challenges their utility for modeling development and disease in a controlled fashion, this stage is well-suited for studies of early human retinogenesis. However, developmentally abnormal events that occur at this stage should also be taken into account, including ectopic deposition of PRs within the INL and the aforementioned demise of RGCs.

At the onset of stage 3, retinal organoids have attained an advanced state of PR development and organization, including formation of IS, OS and an ONL and OPL, making this stage optimal for modeling PR-based diseases. The presence of an OLM is also useful for investigating apical penetration of drug and gene delivery systems to PR cell bodies, given the correspondence of the surrounding culture medium to the anatomical subretinal space (Gonzalez-Cordero et al., 2018). However, PRs are also aberrantly located within the inner regions of stage 3 organoids where they lack ONL-like organization and are less accessible to culture

Development (2019) 146, dev171686. doi:10.1242/dev.171686

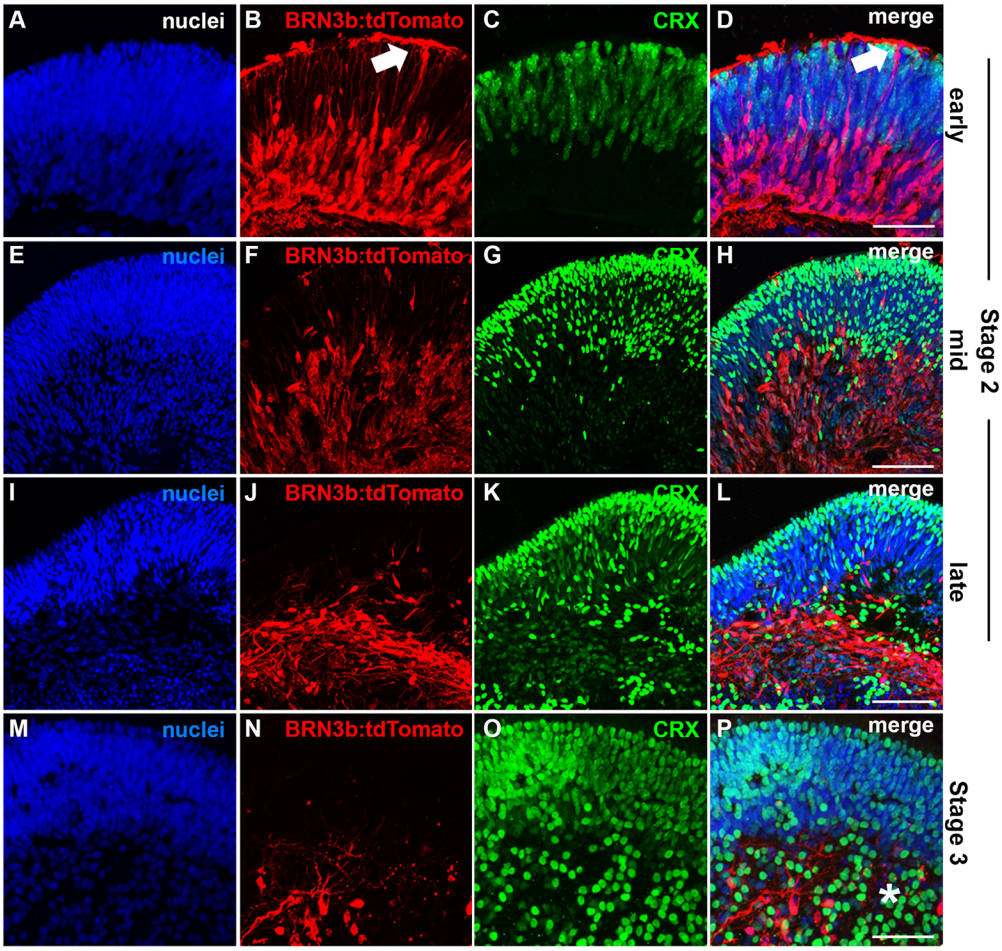

Fig. 8. Time course of RGC loss in stage 2 and stage 3 organoids. (A-D) ICC images of a stage 2 (d55) BRN3b-tdTomato RGC reporter hiPSC line showing an internal layer of RGCs (B) that send projections through the developing outer CRX$^+$ PR layer (C) to the organoid surface (arrows in B and D). (E-P) An identical confocal image analysis was also performed on d90 stage 2 organoids (E-H), d120 stage 2 organoids (I-L) and d160 stage 3 organoids (M-P). Note the loss of tdTomato$^+$ RGC surface projections and overall reduction in RGCs over time, concomitant with an increase in CRX$^+$ PRs in both the ONL and the inner portion of organoids where RGCs persist (asterisk in P). Scale bars: 50 µm.

manipulations. Although these misplaced PRs mature and express opsins, it is unclear whether they develop equivalently to PRs within the well-defined organoid ONL. Even PR subtypes within the ONL do not differentiate in complete synchrony, as demonstrated by the asymmetric surface distribution of rod opsin on individual organoids (Fig. 5H, Fig. S6B,C). Therefore, despite the generally high level of PR differentiation at stage 3, some variability still exists and should be taken into account when controlling for and interpreting organoid studies.

In addition to characterizing organoids within a particular stage, it is important to consider that organoids from consecutive stages can co-exist in the same culture, and that not all organoids achieve stage 3 (Fig. S1D). Therefore, comparative studies of bulk hiPSC retinal organoid populations aligned only by days of differentiation are at increased risk of artifact owing to unaccounted differences in structure, composition and/or maturation. Even the use of isogenic controls does not eliminate this concern, as variabilities were found among cultures differentiated from the same hPSC line.

The aforementioned inconsistencies and shortcomings of retinal organoid cultures are understandable given the stark differences between the *in vitro* and *in vivo* environments. In truth, it is extraordinary that so much of human retinogenesis can be recapitulated in a dish in the absence of multiple events and influences that occur in the developing embryo. For example, isolated hPSC-derived retinal organoids do not form a true optic cup or possess a properly localized RPE layer, nor do they remain attached to forebrain or other developmentally relevant non-retinal lineages. In addition, there is no inner retinal vasculature or migration of astrocytes into the inner retina. Despite the added complexity it would introduce, improvements in retinal organoid technology may come from the inclusion of one or more of these elements into culture systems. For example, co-culture of organoids with RPE could lead to enhanced OS disk morphogenesis and PR function, whereas incorporation of exogenously produced astrocytes might stabilize inner retinal architecture through formation of an ILM. Similarly, maintenance of retina-forebrain connections might facilitate RGC survival and formation of an optic nerve-like structure. It is also important to consider that the human retina has a dual blood supply. Whereas the avascular outer retina is supported by diffusion, the inner retina requires a separate inner retinal microvasculature for long-term survival that is not present in organoids. Therefore, limited diffusion and inadequate internal metabolic support could partially explain the preferential maintenance of outer versus inner retina structure in stage 2 and 3 organoids.

In summary, 3D hPSC retinal organoid technology is a powerful tool that can yield unique insights into human retinal development and disease, and facilitate development of therapies for blinding disorders. However, like all tools, organoids should be employed with careful consideration of both their strengths and limitations. Current strengths of pure retinal organoid cultures relate predominantly to the maturation of PRs and the outer retina, whereas shortcomings stem mostly from progressive disorganization and decay of inner retinal cells and structures. Because neither of these processes obeys a strict timeline, even among organoids from the same culture, we advocate use of a practical, LM-based staging and sorting system to minimize

Development (2019) 146, dev171686. doi:10.1242/dev.171686

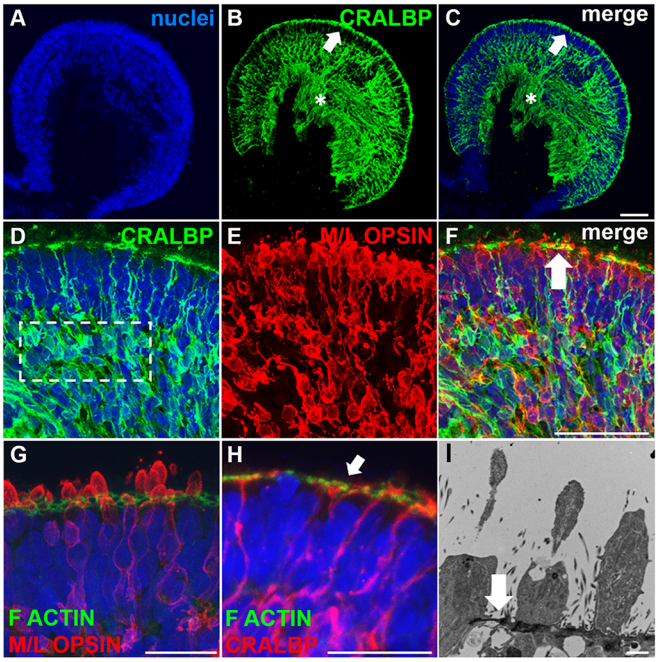

Fig. 9. Outwardly directed MG processes form a discrete OLM-like structure in stage 3 organoids. (A-C) ICC images of a d240 stage 3 organoid showing CRALBP$^+$ MG deep to the ONL that extend processes externally that form a discrete layer (arrow in B and C), whereas inwardly directed MG processes fill the core of the organoid in a disorganized fashion (asterisk in B and C). (D-F) ICC analysis of a d236 stage 3 organoid revealing the presence of CRALBP$^+$ MG cell bodies within the INL (dashed box in D). The CRALBP$^+$ OLM (arrow in F) is situated between the inner and outer segments of M/L-opsin$^+$ cones (E; merge in F). (G,H) ICC image of d200 (G) and d160 (H) stage 3 organoids showing F-actin immunostaining within the OLM (arrow in H) that surrounds M/L-opsin$^+$ cone inner segments (G) and colocalizes with CRALBP (H). (I) Electron micrograph of a d210 stage 3 organoid demonstrating an electron dense OLM-like structure (arrow) relative to PR inner segments. Scale bars: 50 µm (A-F); 25 µm (G,H); 1 µm (I).

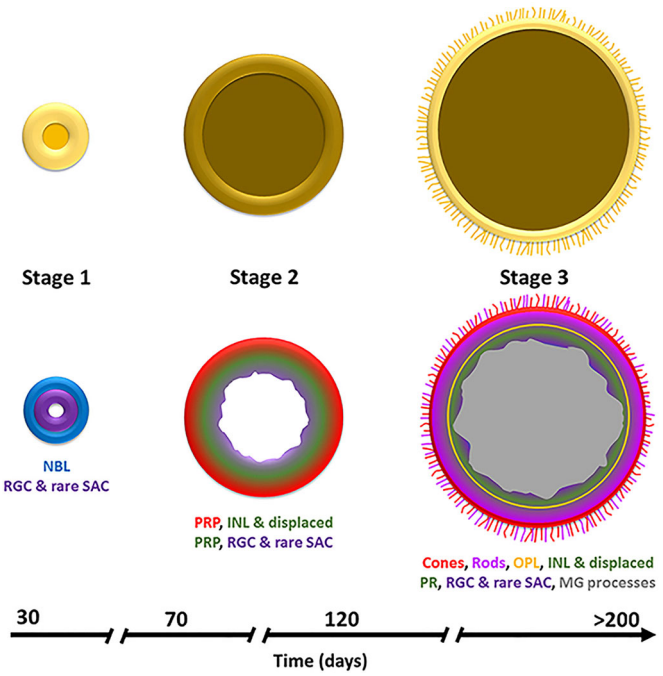

Fig. 10. Summary illustration of the three observed morphological stages of hPSC-derived retinal organoid differentiation. Diagram showing the light microscopic appearance and corresponding cellular composition and lamination of stage 1, 2 and 3 organoids relative to the timeline of differentiation.

intra- and inter-culture variability. Even if the particular stages we describe are not universally applicable to all 3D culture protocols, it is prudent for investigators to establish their own morphological criteria as an added control when utilizing retinal organoids.

MATERIALS AND METHODS

hPSC culture and retinal differentiation

Human PSCs were maintained in 6-well plates on Matrigel (Thermo Fisher). E8, mTeSR1 or StemFlex (WiCell or Thermo Fisher) media were all successfully used to maintain the health and pluripotency of the hPSCs and either Versene (Thermo Fisher) or ReLeSR (STEMCELL Technologies) were used for passaging. Embryoid bodies (EBs) were lifted with 2 mg/ml dispase (Thermo Fisher) or 0.7 ml/well ReLeSR and weaned into Neural Induction Medium [NIM; DMEM:F12 1:1, 1% N2 supplement, 1× MEM nonessential amino acids (MEM NEAA), 1× GlutaMAX (Thermo Fisher) and 2 mg/ml heparin (Sigma)] over the course of 4 days. On day (d) 6, 1.5 nM BMP4 (R&D Systems) was added to fresh NIM and on d7 EBs were plated on Matrigel at a density of 200 EBs per well of a 6-well plate. Half the media was replaced with fresh NIM on d9, d12 and d15 to gradually dilute the BMP4, and on d16 the media was changed to Retinal Differentiation Medium [RDM; DMEM:F12 3:1, 2% B27 supplement, MEM NEAA, 1× antibiotic, anti-mycotic (Thermo Fisher) and 1× GlutaMAX]. On d25-30, 3D OVs became apparent and were dissected with a MSP ophthalmic surgical knife (Surgical Specialties Corporation). Organoids were maintained in poly-HEMA-coated flasks (polyHEMA from Sigma) with twice-weekly feeding of 3D-RDM [DMEM:F12 3:1, 2% B27 supplement, 1× MEM NEAA, 1× antibiotic, anti-mycotic, and 1× GlutaMAX with 5% FBS, 100 µM taurine, 1:1000 chemically defined lipid supplement (11905031, Thermo Fisher)] to which 1 µM all-trans retinoic acid (Sigma) was added until d100, at which point it was removed to enhance outer segment formation. Live cultures were imaged on a Nikon Ts2-FL equipped with a DS-Fi3 camera or on a Nikon Ts100 equipped with a QImaging CE CCD camera. All plasticware and reagents were from Thermo Fisher unless otherwise stated.

Validation of BMP4 treatment

To verify the effects of BMP4 treatment, seven different hiPSC lines were maintained in hPSC medium (DMEM:F12 1:1, 20% KOSR, 1× MEM NEAA, 1× GlutaMAX, 0.8% β-mercaptoethanol and 100 ng/ml bFGF) on irradiated MEF feeder layers (WiCell). EBs were lifted with 2 mg/ml dispase (Thermo Fisher) in EB media (hPSC media without FGF), switched to NIM on d4, and divided into two groups on d6, one treated with 1.5 nM BMP4 and the other treated with vehicle alone. EBs were plated on laminin on d7, and on d16 organoids were harvested in RDM. On d25, retinal organoids and anterior forebrain organoids were counted and the fold increase in retinal organoids was calculated for BMP4 relative to untreated cultures. The *P*-value was calculated based on the average fold difference for all seven lines using Graph-Pad Prism 6 and a one-sample Student's *t*-test against a hypothetical mean of 1.

Cell lines

Table 1 lists the source and derivation method for the 12 hiPSC and four hESC lines used. Nine hiPSC lines were obtained as custom MyCell products from Cellular Dynamics International (now Fujifilm Cellular Dynamics). Tissue samples were obtained with written informed consent in adherence with the Declaration of Helsinki, and with approval from the institutional review board at the University of Wisconsin-Madison. Three hiPSC lines were simultaneously reprogrammed and gene edited from normal fibroblasts acquired from the American Type Culture Collection (Howden et al., 2015); two hESC reporter lines were gene edited by the Waisman Center gene editing core (University of Wisconsin-Madison); one reporter line was gene edited in the lab of Dr Donald Zack (Sluch et al., 2017) and WA09 was obtained from WiCell. All lines were karyotyped,

Development (2019) 146, dev171686. doi:10.1242/dev.171686

tested for pluripotency marker expression by ICC and genotyped to confirm identity before initiation of experiments. Off-target analysis was completed for the top ten off-target sites for each gRNA used for all lines that were CRISPR/Cas9 gene-edited and no indels were detected.

Immunocytochemistry

Organoids were fixed in 4% paraformaldehyde (Electron Microscopy Sciences) at room temperature (RT) with gentle agitation for 35-60 min and washed with PBS before cryopreservation by sinking in 15% sucrose in PBS followed by equilibration in 30% sucrose. They were cryosectioned (15- or 30-µm sections), blocked in 10% normal donkey serum (NDS), 5% bovine serum albumin, 1% fish gelatin and 0.5% Triton X-100 for 1 hour at RT, and incubated with primary antibody at 4°C overnight. See Table S1 for a list of primary antibodies, sources and concentrations. Sections were incubated with species-specific, fluorophore-conjugated secondary antibodies at 1:500 for 30 min in the dark at RT (Alexa Fluor 488, AF546 and AF647; Thermo Fisher). Samples were imaged on a Nikon A1R-Si laser scanning confocal microscope. Manual cone and rod counts were performed on six random images from three to six different organoids from three different lines using Nikon Elements D annotations and measurements module. *P*-values were calculated with an unpaired two-tailed Student's *t*-test (Mann–Whitney test) using Graph-Pad Prism 6.

Multi-photon imaging

For immunolabeled multi-photon imaging, organoids were fixed for 1 h at RT in 4% paraformaldehyde and blocked overnight at 4°C in 10% NDS, 1% Triton X-100 in PBS. Primary antibodies (1:500 rabbit anti-M/L-opsin and 1:100 mouse anti-rod opsin clone 4D2; Millipore) were diluted in NDS/Triton X-100 and organoids were incubated with gentle rocking for 2 days at 4°C. Primary antibody solution was removed and organoids were washed at RT with 1% Triton X-100 in PBS, 3×1 h followed by 3×10 min. Secondary antibodies (donkey anti-mouse AF488 and donkey anti-rabbit AF546) were diluted 1:1000 in 10% NDS/1% Triton X-100 in PBS and organoids were incubated in the dark at 4°C for 2 days. Organoids were washed as above and incubated overnight at 4°C with DAPI or Nuclear ID (ENZO Lifesciences) to counterstain nuclei, followed by washing at RT in the dark as above. Organoids were imaged on a Nikon A1R MP at 850 nm excitation using an Apochromat 25×W MP1300 objective with a numerical aperture of 1.10 and a working distance of 2.0 mm, or a Leica SP8 DIVE at 800 nm excitation using an HC PL IRAPO 25× water objective with a numerical aperture of 1.00. For Fig. S6B, individual tiles were acquired and stitched using Leica LAS X and the Navigator acquisition/tile-scan extension. Projection images for Fig. 5H and movies were assembled using Imaris software v9.1.2 (Bitplane). Live organoid autofluorescence intensity imaging was conducted on a multi-photon fluorescence microscope (Bruker Nano) built around a Nikon Ti:E inverted microscope using a 20× water-immersion objective (Zeiss) with a numerical aperture of 1. A titanium:sapphire (Chameleon Ultra II, Coherent) laser was used for excitation (750 nm) of endogenous fluorophores [e.g. NAD(P)H, retinol, retinoic acid]. A 400-480 nm bandpass filter isolated NAD(P)H fluorescence emission. A 500 nm high pass dichroic mirror and a 500-600 nm bandpass filter isolated retinol/retinoic acid fluorescence emission. Both NAD(P)H and retinol/retinoic acid fluorescence emission were detected simultaneously with two GaAsP photo-multiplier tubes.

TEM

Organoids were fixed in 3% glutaraldehyde and 1% paraformaldehyde in 0.08 M sodium cacodylate buffer (all from Electron Microscopy Sciences) overnight with gentle rocking at 4°C, washed with 0.1 M cacodylate buffer, and post-fixed in 1% osmium tetroxide for 2 h at RT. The organoids were then dehydrated in a graded ethanol series, further dehydrated in propylene oxide and embedded in Epon epoxy resin. Semi-thin (1 µm) and ultra-thin sections were cut with a Leica EM UC6 ultramicrotome and the latter were collected on pioloform-coated (Ted Pella, 19244) one-hole slot grids. Sections were contrasted with Reynolds lead citrate and 8% uranyl acetate in 50% ethanol and imaged on a Philips CM120 electron microscope equipped with an AMT BioSprint side-mounted digital camera and AMT Capture Engine software.

OCT

OCT was performed on live organoids using a commercial Telesto-II spectral domain OCT imaging system (Thorlabs) with 1310 nm light source (superluminescent diode) and objectives (LSM02, *f* # 4.5, NA 0.11 and LSM03, *f* # 9, NA 0.055), and a 2048-element linear InGaAs array-based spectrometer. Images and movies were compiled using the open source 3D-rendering software, Clear Volume (Royer et al., 2015).

Acknowledgements

We are grateful for assistance from the Electron Microscope Facility at the University of Wisconsin-Madison. The authors also thank Prof. Paul Layer (Technische Universität Darmstadt, Germany) for helpful discussions on inner retinal anatomy and starburst amacrine cells.

Competing interests

D.M.G. and M.J.P. have an ownership interest in Opsis Therapeutics LLC, which has licensed the technology to generate optic vesicles from pluripotent stem cell sources reported in this publication. D.M.G. also declared intellectual rights through the Wisconsin Alumni Research Foundation and a consultant role with FUJIFILM Cellular Dynamics International. All other authors indicated no potential conflicts of interest.

Author contributions

Conceptualization: E.E.C., K.S., S.J.M., M.J.P., I.P., J.S., D.S., M.C.S., D.M.G.; Methodology: E.E.C., K.S., S.J.M., M.J.P., I.P., S.E.H., J.S., A.D.J., K.L.E., L.D.J., D.S., V.M.S., X.C., D.J.Z., D.M.G.; Validation: E.E.C., D.M.G.; Investigation: E.E.C., K.S., S.J.M., M.J.P., I.P., S.E.H., J.S., A.D.J., K.L.E., L.D.J., K.B., R.V., Z.E., A.H.; Resources: S.E.H., V.M.S., X.C., D.J.Z.; Writing - original draft: E.E.C., D.M.G.; Writing - review & editing: K.S., M.J.P., R.V., D.S., D.J.Z., M.C.S.; Visualization: E.E.C., D.M.G.; Supervision: E.E.C., D.M.G.; Funding acquisition: K.S., M.C.S., D.M.G.

Funding

This work was supported by grants from the Foundation Fighting Blindness, Research to Prevent Blindness, the National Eye Institute [2R01EY021218-06A1 to D.M.G.] and the National Science Foundation [CBET-1642287 to M.C.S.]; the Sandra Lemke Trout Chair in Eye Research (awarded to D.M.G.); and the Morgridge Interdisciplinary Postdoctoral Fellowship (awarded to K.S.). In addition, this work was supported in part by a core grant to the Waisman Center from the National Institute of Child Health and Human Development [U54 HD090256], and a UW2020 Grant awarded to Anita Bhattacharyya and Su-Chun Zhang by the University of Wisconsin-Madison and the Wisconsin Alumni Research Foundation. Deposited in PMC for release after 12 months.

Supplementary information

Supplementary information available online at
http://dev.biologists.org/lookup/doi/10.1242/dev.171686.supplemental

References

Arno, G., Agrawal, S. A., Eblimit, A., Bellingham, J., Xu, M., Wang, F., Chakarova, D., Parfitt, D. A., Lane, A., Burgoyne, T. et al. (2016). Mutations in *REEP6* cause autosomal-recessive retinitis pigmentosa. *Am. J. Hum. Genet.* **99**, 1305-1315.

Barnea-Cramer, A. O., Wang, W., Lu, S.-J., Singh, M. S., Luo, C., Huo, H., McClements, M. E., Barnard, A. R., MacLaren, R. E. and Lanza, R. (2016). Function of human pluripotent stem cell-derived photoreceptor progenitors in blind mice. *Sci. Rep.* **6**, 29784-29799.

Baye, L. M. and Link, B. A. (2007). Interkinetic nuclear migration and the selection of neurogenic cell divisions during vertebrate retinogenesis. *J. Neurosci.* **27**, 10143-10152.

Bharti, K., Miller, S. S. and Arnheiter, H. (2011). The new paradigm: retinal pigment epithelium cells generated from embryonic or induced pluripotent stem cells. *Pigment Cell Melanoma Res.* **24**, 21-34.

Browne, A. W., Arnesano, C., Harutyunyan, N., Khuu, T., Martinez, J. C., Pollack, H. A., Koos, D. S., Lee, T. C., Fraser, S. E., Moats, R. A. et al. (2017). Structural and functional characterization of human stem-cell-derived retinal organoids by live imaging. *Invest. Ophthalmol. Vis. Sci.* **58**, 3311-3318.

Chao, J. R., Lamba, D. A., Klesert, T. R., La Torre, A., Hoshino, A., Taylor, R. J., Jayabalu, A., Engel, A. L., Khuu, T. H., Wang, R. K. et al. (2017). Transplantation of human embryonic stem cell-derived retinal cells into the subretinal space of a non-human primate. *Trans. Vis. Sci. Tech.* **6**, 1-13.

Choi, J., Lee, S., Mallard, W., Clement, K., Tagliazucchi, G. M., Lim, H., Choi, I. Y., Ferrari, F., Tsankov, A. M., Pop, R. et al. (2015). A comparison of genetically matched cell lines reveals the equivalence of human iPSCs and ESCs. *Nat. Biotechnol.* **33**, 1173-1181.

Deng, W.-L., Gao, M.-L., Lei, X.-L., Lv, J.-N., Zhao, H., He, K.-W., Xia, X.-X., Li, L.-Y., Chen, Y.-C., Li, Y.-P. et al. (2018). Gene correction reverses ciliopathy and photoreceptor loss in iPSC-derived retinal organoids from retinitis pigmentosa patients. *Stem Cell Rep.* **10**, 1267-1281.

Famiglietti, E. V. Jr, (1983). 'Starburst' amacrine cells and cholinergic neurons: mirror-symmetric ON and OFF amacrine cells of rabbit retina. *Brain Res.* **261**, 138-144.

Gagliardi, G., Ben M'Barek, K., Chaffiol, A., Slembrouck-Brec, A., Conart, J.-B., Nanteau, C., Rabesandratana, O., Sahel, J.-A., Duebel, J., Orieux, G. et al. (2018). Characterization and transplantation of CD73-positive photoreceptors isolated from human iPSC-derived retinal organoids. *Stem Cell Rep.* **11**, 665-680.

Gonzalez-Cordero, A., Kruczek, K., Naeem, A., Fernando, M., Kloc, M., Ribeiro, J., Goh, D., Duran, Y., Blackford, S. J. I., Abelleira-Hervas, L. et al. (2017). Recapitulation of human retinal development from human pluripotent stem cells generates transplantable populations of cone photoreceptors. *Stem Cell Reports* **9**, 820-837.

Gonzalez-Cordero, A., Goh, D., Kruczek, K., Naeem, A., Fernando, M., Kleine Holthaus, S.-M., Takaaki, M., Blackford, S. J. I., Kloc, M., Agundez, L. et al. (2018). Assessment of AAV vector tropisms for mouse and human pluripotent stem cell-derived RPE and photoreceptor cells. *Hum. Gene Ther.* **29**, 1124-1139.

Hallam, E., Hilgen, G., Dorgau, B., Zhu, L., Yu, M., Bojic, S., Hewitt, P., Schmitt, M., Uteng, M., Kustermann, S. et al. (2018). Human induced pluripotent stem cells generate light responsive retinal organoids with variable and nutrient dependent efficiency. *Stem Cells* **36**, 1535-1551.

Hambright, D., Park, K.-Y., Brooks, M., McKay, R., Swaroop, A. and Nasonkin, I. O. (2012). Long-term survival and differentiation of retinal neurons derived from human embryonic stem cell lines in un-immunosuppressed mouse retina. *Mol. Vis.* **18**, 920-936.

Howden, S. E., Maufort, J. P., Duffin, B. M., Elefanty, A. G., Stanley, E. G. and Thomson, J. A. (2015). Simultaneous reprogramming and gene correction of patient fibroblasts. *Stem Cell Rep.* **5**, 1-10.

Iraha, S., Tu, H.-Y., Yamasaki, S., Kagawa, T., Goto, M., Takahashi, R., Watanabe, T., Sugita, S., Yonemura, S., Sunagawa, G. A. et al. (2018). Establishment of immunodeficient retinal degeneration model mice and functional maturation of human ESC-derived retinal sheets after transplantation. *Stem Cell Rep.* **10**, 1059-1074.

Jin, Z.-B., Okamoto, S., Xiang, P. and Takahashi, M. (2012). Integration-free induced pluripotent stem cells derived from retinitis pigmentosa patient for disease modeling. *Stem Cells Transl. Med.* **1**, 503-509.

Kobayashi, W., Onishi, A., Tu, H.-Y., Takihara, Y., Matsumura, M., Tsujimoto, K., Inatani, M., Nakazawa, T. and Takahashi, M. (2018). Culture systems of dissociated mouse and human pluripotent stem cell-derived retinal ganglion cells purified by two-step immunopanning. *Invest. Ophthalmol. Vis. Sci.* **59**, 776-787.

Kuwahara, A., Ozone, C., Nakano, T., Saito, K., Eiraku, M. and Sasai, Y. (2015). Generation of a ciliary margin-like stem cell niche from self-organizing human retinal tissue. *Nat. Commun.* **6**, 6286-6301.

Lakowski, J., Welby, E., Budinger, D., Di Marco, F., Di Foggia, V., Bainbridge, J. W. B., Wallace, K., Gamm, D. M., Ali, R. R. and Sowden, J. C. (2018). Isolation of human photoreceptor precursors via a cell surface marker panel from stem cell-derived retinal organoids and fetal retinae. *Stem Cells* **36**, 709-722.

Lamba, D. A., Gust, J. and Reh, T. A. (2009). Transplantation of human embryonic stem cell-derived photoreceptors restores some visual function in *Crx*-deficient mice. *Cell Stem Cell* **4**, 73-79.

Lamba, D. A., McUsic, A., Hirata, R. K., Wang, P.-R., Russell, D. and Reh, T. A. (2010). Generation, purification and transplantation of photoreceptors derived from human induced pluripotent stem cells. *PLoS ONE* **5**, e8763.

Langer, K. B., Ohlemacher, S. K., Phillips, M. J., Fligor, C. M., Jiang, P., Gamm, D. M. and Meyer, J. S. (2018). Retinal ganglion cell diversity and subtype specification from human pluripotent stem cells. *Stem Cell Rep.* **10**, 1282-1293.

Lowe, A., Harris, R., Bhansali, P., Cvekl, A. and Liu, W. (2016). Intercellular adhesion-dependent cell survival and ROCK-regulated actomyosin-driven forces mediate self-formation of a retinal organoid. *Stem Cell Rep.* **6**, 743-756.

Luo, Z., Zhong, X., Li, K., Xie, B., Liu, Y., Ye, M., Li, K., Xu, C. and Ge, J. (2018). An optimized system for effective derivation of three-dimensional retinal tissue via Wnt signaling regulation. *Stem Cells* **36**, 1709-1722.

Mandai, M., Fujii, M., Hashiguchi, T., Sunagawa, G. A., Ito, S., Sun, J., Kaneko, J., Sho, J., Yamada, C. and Takahashi, M. (2017). iPSC-derived retina transplants improve vision in *rd1* end-stage retinal-degeneration mice. *Stem Cell Rep.* **8**, 69-83.

McLelland, B. T., Lin, B., Mathur, A., Aramant, R. B., Thomas, B. B., Nistor, G., Keirstead, H. S. and Seiler, M. J. (2018). Transplanted hESC-derived retina organoid sheets differentiate, integrate, and improve visual function in retinal degenerate rats. *Invest. Ophthalmol. Vis. Res.* **59**, 2586-2603.

Megaw, R., Abu-Arafeh, H., Jungnickel, M., Mellough, C., Gurniak, C., Witke, W., Zhang, W., Khanna, H., Mill, P., Dhillon, B. et al. (2017). Gelsolin dysfunction causes photoreceptor loss in induced pluripotent cell and animal retinitis pigmentosa models. *Nat. Commun.* **8**, 271-281.

Mellough, C. B., Collin, J. Khazim, M., White, K., Sernagor, E., Steel, D. H. W. and Lako, M. (2015). IGF-1 signaling plays an important role in the formation of three-dimensional laminated neural retina and other ocular structures from human embryonic stem cells. *Stem Cells* **33**, 2416-2430.

Meyer, J. S., Shearer, R. L., Capowski, E. E., Wright, L. S., Wallace, K. A., McMillan, E. L., Zhang, S.-C. and Gamm, D. M. (2009). Modeling early retinal development with human embryonic and induced pluripotent stem cells. *Proc. Natl. Acad. Sci. USA* **106**, 16698-16703.

Meyer, J. S., Howden, S. E., Wallace, K. A., Verhoeven, A. D., Wright, L. S., Capowski, E. E., Pinilla, I., Martin, J. M., Tian, S., Stewart, R. et al. (2011). Optic vesicle-like structures derived from human pluripotent stem cells facilitate a customized approach to retinal disease treatment. *Stem Cells* **29**, 1206-1218.

Miyagishima, K. J., Wan, Q., Corneo, B., Sharma, R., Lofti, M. R., Boles, N. C., Hua, F., Maminishkis, A., Zhang, C., Blenkinsop, T. et al. (2016). In pursuit of authenticity: induced pluripotent stem cell-derived retinal pigment epithelium for clinical applications. *Stem Cells Transl. Med.* **5**, 1562-1574.

Nakano, T., Ando, S., Takata, N., Kawada, M., Muguruma, K., Sekiguchi, K., Saito, K., Yonemura, S., Eiraku, M. and Sasai, Y. (2012). Self-formation of optic cups and storable stratified neural retina from human ESCs. *Cell Stem Cell* **10**, 771-785.

Nazor, K. L., Altun, G., Lynch, C., Tran, H., Harness, J. V., Slavin, I., Garitaonandia, I., Müller, F.-J., Wang, Y.-C., Boscolo, F. S. et al. (2012). Recurrent variations in DNA methylation in human pluripotent stem cells and their differentiated derivatives. *Cell Stem Cell* **10**, 620-634.

Osterberg, G. (1935). Topography of the layers of rods and cones in the human retina. *Acta Ophthalmol. Suppl.* **6**, 1-103.

Ovando-Roche, P., West, E. L., Branch, M. J., Sampson, R. D., Fernando, M., Munro, P., Georgiadis, A., Rizzi, M., Kloc, M., Naeem, A. et al. (2018). Use of bioreactors for culturing human retinal organoids improves photoreceptor yields. *Stem Cell Res. Ther.* **9**, 156-170.

Parfitt, D. A., Lane, A., Ramsden, C. M., Carr, A.-J. F., Munro, P. M., Jovanovic, K., Schwarz, N., Kanuga, N., Muthiah, M. N., Hull, S. et al. (2016). Identification and correction of mechanisms underlying inherited blindness in human iPSC-derived optic cups. *Cell Stem Cell* **18**, 769-781.

Phillips, M. J., Wallace, K. A., Dickerson, S. J., Miller, M. J., Verhoeven, A. D., Martin, J. M., Wright, L. S., Shen, W., Capowski, E. E., Percin, E. F. et al. (2012). Blood-derived human iPS cells generate optic vesicle-like structures with the capacity to form retinal laminae and develop synapses. *Invest. Ophthalmol. Vis. Sci.* **53**, 2007-2019.

Phillips, M. J., Perez, E. T., Martin, J. M., Reshel, S. T., Wallace, K. A., Capowski, E. E., Singh, R., Wright, L. S., Clark, E. M., Barney, P. M. et al. (2014). Modeling human retinal development with patient-specific induced pluripotent stem cells reveals multiple roles for Visual System Homeobox 2. *Stem Cells* **32**, 1480-1492.

Phillips, M. J., Jiang, P., Howden, S., Barney, P., Min, J., York, N. W., Chu, L.-F., Capowski, E. E., Cash, A., Jain, S. et al. (2018a). A novel approach to single cell RNA-sequence analysis facilitates in silico gene reporting of human pluripotent stem cell-derived retinal cell types. *Stem Cells* **36**, 313-324.

Phillips, M. J., Capowski, E. E., Petersen, A., Jansen, A. D., Barlow, K., Edwards, K. L. and Gamm, D. M. (2018b). Generation of a rod-specific NRL reporter line in human pluripotent stem cells. *Sci. Rep.* **8**, 2370-2381.

Reichman, S., Terray, A., Slembrouck, A., Nanteau, C., Orieux, C. G., Habelerd, W., Nandrot, E. F., Sahel, J.-A., Monvilled, C. and Goureau, O. (2014). From confluent human iPS cells to self-forming neural retina and retinal pigment epithelium. *Proc. Natl. Acad. Sci. USA* **111**, 8518-8523.

Rodieck, R. W. and Marshak, D. W. (1992). Spatial density and distribution of choline acetyltransferase immunoreactive cells in human, macaque, and baboon retinas. *J. Comp. Neurol.* **321**, 46-64.

Royer, L. A., Weigert, M., Günther, U., Maghelli, N., Jug, F., Sbalzarini, I. F. and Myers, E. W. (2015). ClearVolume: open-source live 3D visualization for light-sheet microscopy. *Nat. Methods* **12**, 480-481.

Schwarz, N., Lane, A., Jovanovic, K., Parfitt, D. A., Aguila, M., Thompson, C. L., da Cruz, L., Coffey, P. J., Chapple, J. P., Hardcastle, A. J. et al. (2017). Arl3 and RP2 regulate the trafficking of ciliary tip kinesins. *Hum. Mol. Genet.* **26**, 2480-2492.

Sharma, T. P., Wiley, L. A., Whitmore, S. S., Anfinson, K. R., Cranston, C. M., Oppedal, D. J., Daggett, H. T., Mullins, R. F., Tucker, B. A. and Stone, E. M. (2017). Patient-specific induced pluripotent stem cells to evaluate the pathophysiology of *TRNT1*-associated retinitis pigmentosa. *Stem Cell Res.* **21**, 58-70.

Shimada, H., Lu, Q., Insinna-Kettenhofen, C., Nagashima, K., English, M. A., Semler, E. M., Mahgerefteh, J., Cideciyan, A. V., Li, T., Brooks, B. P. et al. (2017). *In vitro* modeling using ciliopathy-patient-derived cells reveals distinct cilia dysfunctions caused by *CEP290* mutations. *Cell Rep.* **20**, 384-396.

Shirai, H., Mandai, M., Matsushita, K., Kuwahara, A., Yonemura, S., Nakano, T., Assawachananont, J., Kimura, T., Saito, K., Terasaki, H. et al. (2016). Transplantation of human embryonic stem cell-derived retinal tissue in two primate models of retinal degeneration. *Proc. Natl. Acad. Sci. USA* **113**, E81-E90.

Singh, R., Phillips, M. J., Kuai, D., Meyer, J., Martin, J. M., Smith, M. A., Perez, E. T., Shen, W., Wallace, K. A., Capowski, E. E. et al. (2013). Functional analysis of serially expanded human iPS cell-derived RPE cultures. *Invest. Ophthalmol. Vis. Sci.* **54**, 6767-6778.

Singh, R. K., Mallela, R. K., Cornuet, P. K., Reifler, A. N., Chervenak, A. P., West, M. D., Wong, K. Y. and Nasonkin, I. O. (2015). Characterization of three-dimensional retinal tissue derived from human embryonic stem cells in adherent monolayer cultures. *Stem Cells Dev.* **24**, 2778-2795.

Sluch, V. M., Chamling, X., Liu, M. M., Berlinicke, C. A., Cheng, J., Mitchell, K. L., Welsbie, D. S. and Zack, D. J. (2017). Enhanced stem cell differentiation and immunopurification of genome engineered human retinal ganglion cells. *Stem Cells Transl. Med.* **6**, 1972-1986.

Sridhar, A., Ohlemacher, S. K., Langer, K. B. and Meyer, J. S. (2016). Robust differentiation of mRNA-reprogrammed human induced pluripotent stem cells toward a retinal lineage. *Stem Cells Transl. Med.* **5**, 417-426.

Tucker, B. A., Scheetz, T. E., Mullins, R. F., DeLuca, A. P., Hoffmann, J. M., Johnston, R. M., Jacobson, S. G., Sheffield, V. C. and Stone, E. M. (2011). Exome sequencing and analysis of induced pluripotent stem cells identify the cilia-related gene male germ cell-associated kinase (MAK) as a cause of retinitis pigmentosa. *Proc. Natl. Acad. Sci. USA* **108**, E569-E576.

Tucker, B. A., Mullins, R. F., Streb, L. M., Anfinson, K., Eyestone, M. E., Kaalberg, E., Riker, M. J., Drack, A. V., Braun, T. A. and Stone, E. M. (2013). Patient-specific iPSC-derived photoreceptor precursor cells as a means to investigate retinitis pigmentosa. *eLife* **2**, e00824.

Wahlin, K. J., Maruotti, J. A., Sripathi, S. R., Ball, J., Angueyra, J. M., Kim, C., Grebe, R., Li, W., Jones, B. W. and Zack, D. J. (2017). Photoreceptor outer segment-like structures in long-term 3D retinas from human pluripotent stem cells. *Sci. Rep.* **7**, 766-781.

Wiley, L. A., Burnight, E. R., DeLuca, A. P., Anfinson, K. R., Cranston, C. M., Kaalberg, E. E., Penticoff, J. A., Affatigato, L. M., Mullins, R. F., Stone, E. M. et al. (2016). cGMP production of patient-specific iPSCs and photoreceptor precursor cells to treat retinal degenerative blindness. *Sci. Rep.* **6**, 30742-30758.

Yang, T.-C., Chuang, J.-H., Buddhakosai, W., Wu, W.-J., Lee, C.-J., Chen, W.-S., Yang, Y.-P., Li, M.-C., Peng, C.-H. and Chen, S.-J. (2017). Elongation of axon extension for human iPSC-derived retinal ganglion cells by a nano-imprinted scaffold. *Int. J. Mol. Sci.* **18**, 2013-2027.

Yanoff, M. and Duker, J. S. (2013). *Ophthalmology:Expert Consult: Online and Print*. p. 241. Elsevier Health Sciences.

Yoshida, T., Ozawa, Y., Suzuki, K., Yuki, K., Ohyama, M., Akamatsu, W., Matsuzaki, Y., Shimmura, S., Mitani, K., Tsubota, K. et al. (2015). The use of induced pluripotent stem cells to reveal pathogenic gene mutations and explore treatments for retinitis pigmentosa. *Mol. Brain* **7**, 45-56.

Zhong, X., Gutierrez, C., Xue, T., Hampton, C., Vergara, M. N., Cao, L-H., Peters A., Park, T. S., Zambidis, E .T., Meyer, J. S., et al. (2014). Generation of three-dimensional retinal tissue with functional photoreceptors from human iPSCs. *Nat. Commun.* **5**, 4047.

Zhu, J., Cifuentes, H., Reynolds, J. and Lamba, D. A. (2017). Immunosuppression via loss of IL2rγ enhances long-term functional integration of hESC-derived photoreceptors in the mouse retina. *Cell Stem Cell* **20**, 374-384.e5.

Zhu, J., Reynolds, J., Garcia, T., Cifuentes, H., Chew, S., Zeng, X. and Lamba, D. A. (2018). Generation of transplantable retinal photoreceptors from a current good manufacturing practice-manufactured human induced pluripotent stem cell line. *Stem Cells Transl. Med.* **7**, 210-219.